Earth Surf. Dynam. Discuss., 3, 129–171, 2015
www.earth-surf-dynam-discuss.net/3/129/2015/
doi:10.5194/esurfd-3-129-2015

Earth Surface Dynamics Discussions
Open Access

Groundwater seepage landscapes from local or distal sources in experiments and on Mars

W. A. Marra[1], S. J. McLelland[2], D. R. Parsons[2], B. J. Murphy[2], E. Hauber[3], and M. G. Kleinhans[1]

[1]Faculty of Geosciences, Universiteit Utrecht, Heidelberglaan 2, 3584 CS, Utrecht, the Netherlands
[2]Department of Geography, Environment and Earth Sciences, University of Hull, Cottingham Road, Hull, HU6 7RX, UK
[3]Deutsches Zentrum für Luft- und Raumfahrt (DLR), Institut für Planetenforschung, Rutherfordstraße 2, 12489 Berlin, Germany

Received: 4 February 2015 – Accepted: 9 February 2015 – Published: 19 February 2015

Correspondence to: W. A. Marra (w.a.marra@uu.nl)

Published by Copernicus Publications on behalf of the European Geosciences Union.

Abstract

Theater-headed valleys can form due to groundwater sapping, but these valleys could also be the result of knick-point (waterfall) erosion generated by overland flow. This morphological ambiguity hampers the interpretation of such valleys on Mars, especially due to insufficient knowledge of material properties, but the climate implications are quite different. Instead of single-valley morphology, metrics of the entire landscape may provide diagnostic insight in the formative hydrological conditions. However, flow patterns and the resulting landscapes are different for different sources of groundwater and poorly understood. We aim to increase our understanding of the formation of the entire landscapes by sapping from different sources of groundwater and to provide a framework of landscape metrics of such systems to aid interpretation of such landscapes. We study sapping from local and distal sources of groundwater in sandbox experiments and combine our results with previous experiments. Key results are that groundwater piracy acts on distally-fed valleys, which results in a sparsely dissected landscape of many small and a few large valleys while locally-fed valleys result in a densely dissected landscape. In addition, distally-fed valleys grow into the direction of the groundwater source while locally-fed channels grow in a broad range of directions and have a strong tendency to bifurcate, particularly on flat horizontal surfaces. As an example, we apply these results to two Martian cases. The valleys of Louros Valles show properties of sapping by a local source and Nirgal Vallis shows evidence of a distal source, which is likely groundwater from Tharsis.

1 Introduction

Valleys with theater-shaped heads exist in the landscapes of Earth and Mars. On Mars, such valleys are for example Louros Valles (Fig. 1a) and Nirgal Vallis (Harrison and Grimm, 2005). Terrestrial examples can be found in the Atacama Desert in Chile (Fig. 1b), on the Canterbury Plain, New Zealand, on the Colorado plateau and on

ESURFD
3, 129–171, 2015

Hawaii (Schumm and Phillips, 1986; Howard and Kochel, 1988; Craddock et al., 2012). Furthermore, much smaller, but similar in shape are valleys that emerge in riverbanks (Fig. 1c) or those on the beach during a receding tide (Higgins, 1982; Otvos, 1999; Fox and Wilson, 2010; Hagerty, 1991).

The small valleys on the beach and riverbanks form in several hours by seeping of groundwater in unconsolidated sediment. The governing processes and morphology are the same as in groundwater seepage experiments (e.g. Howard and McLane, 1988) and consist of undercutting by erosion by groundwater seepage and resulting head wall collapse. This process is also known to be responsible for the valleys in the Colorado plateau sandstone (e.g. Laity and Malin, 1985), and has long been thought to be the cause of the formation of valleys on Hawaii and on Mars (Kochel and Piper, 1986). However, head-wall retreat due to undercutting by waterfall erosion of a hard cap rock produces similar valley morphology (Lamb et al., 2006) and is probably a better explanation for the theater-headed valleys next to the Snake River in Idaho (Fig. 1d) and the Chilean valleys (Irwin et al., 2014).

The main argument against a groundwater origin of the Martian valleys is the limited erodibility by the low seepage discharge (Lamb et al., 2006), but the material properties of Mars are largely unknown, which hinders unambiguous interpretation of the formative mechanism of the theater-headed valleys. Furthermore, small upstream channels feeding the main valleys are expected for waterfall erosion which are visible in terrestrial cases (e.g., Fig. 1e), but evidence for such a source is missing for many Martian cases. Most importantly, formation by either waterfall erosion or groundwater seepage has quite different implications for the responsible climate conditions, as groundwater puts less constrains on surface conditions to sustain large amounts of liquid water.

Besides the single-valley morphology, the landscape properties of multiple valleys may help in the interpretation of the Martian valleys. An important feedback for groundwater seepage is flow piracy, since valleys are topographic depressions, hence they attract more groundwater from their surrounding, possibly resulting in the abandonment of other valleys (Howard and McLane, 1988). Landscape metrics may provide

ESURFD
3, 129–171, 2015

information on the presence of feedback mechanisms like groundwater piracy. Furthermore, the angle of valley bifurcations, and the orientation of valleys could indicate the responsible hydrological system and the location of the groundwater source (Jaumann and Reiss, 2002; Devauchelle et al., 2012; Glines and Fassett, 2013).

Our knowledge of the groundwater sapping processes and their relation to landscape evolution is rather limited. Particularly as systems with only groundwater processes are absent on Earth and previous experimental studies were mostly limited to the same boundary conditions of groundwater from a constant-head tank (e.g. Howard and McLane, 1988; Lobkovsky et al., 2004; Schorghofer et al., 2004; Pornprommin et al., 2010; Marra et al., 2014a). These experiments simulated a distant groundwater source and showed the basic morphology of sapping valleys, revealing the importance of groundwater piracy as a key process for valley evolution. However, alternate hydrological systems exist where other processes play a role, which results in a different landscape evolution. For example, in contrast to a distant groundwater source, a local groundwater source can release water from a shallow aquifer, generated by local infiltration of precipitation. Such systems exist (Abrams et al., 2009; Fig. 1f) and have been studied in experiments to some extent (Berhanu et al., 2012), but require more attention in terms of their morphological impact on landscape dynamics. We hypothesize that a local groundwater source results in less groundwater flow piracy compared to groundwater that travels some distance, because a local source is less influenced by the regional topographic gradient. Since flow piracy is an important mechanism in the formation of theater-headed valleys by groundwater seepage, we expect a different morphological development for locally-fed sapping valleys.

In this paper, we aim to increase our understanding of groundwater seepage processes, specifically on the resulting valley formation. In order to expand our knowledge on the possible range of processes, we study the difference in morphological development of valleys that emerge from distant and local sources of groundwater in scaled experiments. Furthermore, we combine our experimental insight with previous studies in order to cover a complete range of possible sapping systems. The objective is es-

ESURFD
3, 129–171, 2015

sentially to provide a framework that shows the arrangement of multiple valleys, i.e., the orientation and length distribution that result from different hydrological boundary conditions. These properties will aid in the identification of the formative processes when the single valley morphology is ambiguous, and will constrain the hydrological and climate conditions during formation. As an example, we apply our developed framework to two often-cited cases of groundwater seepage on Mars, Nirgal Vallis and Louros Valles, and relate their landscape metrics to the possible sources of groundwater.

2 Methods

2.1 Experimental design

We conducted several flume experiments in the Total Environmental Simulator (TES) facility at the University of Hull to study the morphological development of theater-headed valleys by seeping groundwater. Moreover, with these experiments we studied the effect of groundwater seepage from a local and from a distal source. We simulated groundwater seeping from a distal source by using a fixed-head groundwater level at the upstream end of the setup. As a local source of groundwater, we applied precipitation on the entire experiment domain, using an intensity lower than the infiltration capacity of the sediment. We repeated both experiments with an idealized initial morphology and with a heterogeneous initial morphology that was the result of a previous experiment. In this section, we present the setup, the initial topography and applied boundary conditions across the experimental set.

The initial idealized morphology consisted of a volume of sand with a median grain size of 0.7 mm, that comprised (1) a flat area of 1.7 m upstream and (2) a slope of $0.22\,\mathrm{m\,m^{-1}}$ for 3.5 m (Fig. 2), which was equal over a width of 4 m. The sloping section ensured seepage of groundwater from a hydrostatic groundwater level, i.e. not pressurized. The sediment was placed on top of a partially sloping impermeable floor to increase groundwater flow in the downstream half of the setup and to reduce the amount

ESURFD
3, 129–171, 2015

of sediment required. This floor was flat for 2.6 m and the slope was 0.11 m m^{-1} for 2.6 m. Pond liner ensured the impermeability of the floor and walls. A rough cloth on top of the pond liner prevented the entire block of sediment from sliding down. The total sediment depth was 0.5 m in the upstream flat part, sloping towards the downstream end. At the downstream end, a row of 6 cm high bricks truncated the wedging slope to prevent the sediment from sliding down. In addition, the small spaces between these 10 cm wide bricks acted as initial surface perturbations. This ensured evenly distributed channel initiation over the entire width of the sediment.

To simulate a groundwater system from a distal source, we used a constant head tank at the upstream end of the setup. This constant head tank was constructed over the entire width of the setup using a 0.6 mm mesh, braced with chicken wire and steel gratings. To simulate a local groundwater system, we used a series of spray nozzles above the setup to supply water over the sediment surface. These nozzles were set to spray at such discharge that the water infiltrated, which corresponds with a discharge lower than the infiltration capacity of the sediment. A rising groundwater table induced seepage, but in contrast to the constant head tank, the seepage areas were fed by locally infiltrated groundwater. Twelve spray nozzles with square spray patterns were used, which were pressurized from a ring main to ensure equal spray rates for all nozzles.

We carried out five experiments with the above described boundary condition combinations (Table 1). Experiment "Distal" was carried out entirely with the constant head tank as boundary condition. The final morphology of this experiment was used as initial morphology of experiment "Local after Distal", which was run with the spray nozzles. Experiments "Local" was run with the spray nozzles on the above-described initial topography. Experiment "Local 2" was only run to generate an initial morphology with the same conditions as "Local", but this experiment was ceased early. The final morphology of "Local 2" was the initial morphology of "Distal after Local", which was subject to groundwater flow from the constant head tank.

ESURFD
3, 129–171, 2015

2.2 Experimental imagery and elevation models

We captured the morphological development of the experiments using time-lapse photography. These images allowed us to study the experiments in detail from different angles. Moreover, we derived channel dimensions from orthorectified time-lapse images. The time-lapse setup consisted of six cameras (Canon PowerShot A640), mounted around the experimental setup (see C1–C6 in Fig. 2), which were synchronously triggered at set intervals. These intervals differed from 30 s to 5 min, based on the pace of the morphological development in the ongoing experiment (values in Table 1).

For each experiment, time-lapse imagery from four angles were processed to a single orthorectified image. Camera's C1, C2, C4 and C5 (Fig. 2) were used to construct orthorectified images. Orthorectification was conducted on the initial surface elevation model. Using the initial surface elevation, the orthorectified images were distorted in morphologically altered areas. However, the dimensions of erosional features, such as the valleys in our experiments, remain correct using this method. We performed time-lapse orthorectification in MATLAB, using the Image Processing Toolbox and the Camera Calibration Toolbox for MATLAB.

For detailed morphological analysis and morphometrical analysis, we collected digital elevation models and orthorectified images at the end of each experiment using a large set of images and a structure-from-motion (SfM) algorithm (Forsyth and Ponce, 2011). In addition, we also acquired these data several times during the Distal and Distal-after-Local experiment at irregular intervals (Table 1).

Elevation models were acquired at the end of each experiment and during the experiments Distal and Distal-after-Local every day of the experiment (see Table 1) using SfM For each elevation model and associated orthorectified image, we took a set of about 70–100 digital images with about 80 % overlap. We took these images by hand, allowing us to capture the area of interest. Twenty-four targets with known coordinates within the experimental setup enabled referencing of the images. Camera positions and orientations were solved using these target coordinates and matched features be-

ESURFD
3, 129–171, 2015

tween images. To increase the quality of the result, we removed features in wet areas in order to eliminate faulty matches in reflective areas due to different lightning angles between images. Elevation models were generated for each set of images, which were processed to a gridded elevation model with 1 mm cell size and a 0.5 mm orthorectified images. We used a Canon 550D DSLR camera with an 18–55 mm f/2.8 lens to take the photos, which we processed in RAW format to 16 bit TIF images to eliminate compression artifacts. We used Agisoft PhotoScan for SFM processing (Agisoft, 2014).

In addition, we used a laser scanner to obtain elevation models at the end of each experiment. Point-cloud elevation data of the final morphology were obtained using a laser scanner from two angles in order to eliminate data shadows outside the line-of-sight of the scanner (see Fig. 2). These point-clouds were oriented using fixed targets in the experimental setup. The combined scans were gridded to 2 mm elevation models. We used a Leica ScanStation 2 laser scanner for data acquisition, CloudCompare for point-cloud orientation and ArcGIS for gridding of the point-cloud data.

2.3 Valley development and eroded volume

The length L (m) and width W (m) of each valley that formed during the experiments were determined for each time-lapse interval from the orthorectified time-lapse images. Valley depth D (m) was defined as the deepest point of each valley, i.e. the largest elevation difference between the original surface and the eroded surface. Valley depth was measured at each SfM interval. The final valley floor slope S_f ($m\,m^{-1}$) was extracted from the final DEM. We defined the valley floor as the lowest point in each valley cross section. We estimated the erosion rates of each valley during the experiments by combining the valley dimensions and valley shapes. First, the eroded volume V (m^3) was estimated as:

$$V = W \cdot L \cdot D \cdot \mathrm{SI_c} \cdot 0.5, \quad (1)$$

for which W and L were taken at each time-lapse interval, D (m) is the channel depth that was interpolated between measurements at each time-lapse interval. $\mathrm{SI_c}$ is the

ESURFD
3, 129–171, 2015

shape-index of the valley cross-section, which is the average ratio of the actual valley cross section to the square cross-section of $W \times D$. The factor 0.5 corrects for the longitudinal profile of the valley, which is in all cases an approximate triangle. Valley volume was transformed to erosion rate E ($\mathrm{g\,s^{-1}}$):

$$E = \frac{\Delta V \rho_s (1-n) \cdot 10^{-3}}{\Delta T}, \quad (2)$$

where ΔV is the change in volume, ρ_s is the density of sand ($2300\,\mathrm{kg\,m^{-1}}$), n the porosity of the sediment (0.3) and ΔT (s) is the time over which the change in volume occurred. Cumulative erosion was compared to sediment output measurements using buckets.

2.4 Martian landscape metrics

We constructed elevation profiles and extracted the orientation in degrees from North of valley segments, the bifurcation angles and valley lengths of Louros Valles and Nirgal Vallis. Channel segments were digitized based on THEMIS Daytime Infrared Mosaic (Fergason et al., 2013) and HRSC (Jaumann et al., 2007) imagery. We distinguished different stream-orders, based on the Hack stream ordering number (Hack, 1957). In this system, the first-order is the main, downstream, valley; the first tributary is the second order and so on. We choose this system since it represents the chronology of valley formation by headward erosion. Elevation profiles were extracted from HRSC image H0380_0001 (125 m resolution DEM) for Louros Valles, valleys of Nirgal Vallis were too small to produce useful profiles.

The dataset of channel segments was transformed to a network-topology to distinguish upstream and downstream direction, using logical operators based on the methods described in Marra et al. (2014d) using ArcGIS and MATLAB. In this dataset, we identified bifurcations, valley heads and outlets based on the topology of the network. From this dataset, the orientation relative to north of each valley segment was extracted

ESURFD
3, 129–171, 2015

for each stream order (building upon the work of Jaumann and Reiss, 2002). Orientation distributions were normalized per stream order to better show the difference and reveal the effect of bifurcations of valley orientation. At each bifurcation, we calculated the bifurcation angle between the upstream channel segments (following Glines and Fassett, 2013). Furthermore, for each valley head in the network, we calculated the distance to the first lower-order valley segment.

What we here refer to as bifurcation is a valley that splits in upstream direction. This definition relates to the chronological order of events in valley formation. In active rivers, the term bifurcation is used for a channel that slits into two channels in downstream direction, which relates to the motion direction of water.

3 Experimental results

In the following section, we first describe the observed morphological development during the experiments, and then we link this morphological development to the acting processes. Time-lapse imagery and elevation models support these observations (time-lapse movies are available in the Supplement.

3.1 Distal groundwater source

The distal groundwater experiment was characterized by slowly developing valleys. This experiment took over three days to complete and was carried out with a constant discharge of 2.4 liter per minute (Table 1).

The sediment saturated in the first hours of the experiment. During this stage, a visible wetting front at the surface progressed from the upstream constant head tank in downstream direction. The sediment became fully saturated at the foot of the slope where seepage occurred after 2.5 h over the full width of the sediment surface (Fig. 3a-i). The initial seepage pattern remained roughly the same, though the seepage area extended upslope to about 1 m from the foot of the slope. Initially, the seepage was

ESURFD
3, 129–171, 2015

too low for fluvial transport to occur. As the seepage rate increased, fluvial transport started after 4 h and the first valleys started to form at the foot of the slope within the seepage area.

The initial valleys that formed at the foot of the slope featured a combination of mass-wasting and fluvial processes. Mass-wasting of saturated sediment at the head caused headward erosion, and fluvial processes removed the material from the valley (Fig. 3a-iii). As the valleys developed in upstream direction, the seepage area retreated and seepage focused within the valleys as shown by drying of the sediment between the valleys and a concurrent increase of discharge within the valleys (Fig. 3a-iii). Seepage was limited to a declining number of valleys, as the valleys that reached furthermost upstream progressively attracted more groundwater. From the ten valleys that started to form in the initial stage of the experiment, only six remained active after a few hours (Fig. 3a-iv), and only three remained active for several days (Fig. 3a-v). The decreasing number of active valleys testifies to the presence of groundwater piracy, which is typical for the process of groundwater sapping. This groundwater piracy resulted in a final morphology comprising a few large and several small valleys (Fig. 4). The valleys did not bifurcate, which is the result of the high initial slope (Pornprommin et al., 2010).

The remaining valleys grew and as they became deeper, the head- and side-walls gained strength by cohesion as the sediment was moist. As a result, the head-wall retreat was governed by collapse due to undercutting at the toe, in contrast to the slumping of the entire valley head before the development of this cohesive top layer. In this process, the toe of the head wall was destabilized by fluvial erosion, resulting in collapse. The collapsed material transformed into a mudflow. Therefore, the collapsed material spread over a distance of 0.1 to 0.2 m into the valleys. Fluvial transport removed this material from the upstream end to the downstream end of the experimental setup. These processes showed a cyclic behavior: head collapse only occurred after a destabilization of the head due to the removal of the sediment by fluvial transport. This cycle is essential for the continuation of the process as the channel head would stabilize without such erosion and sediment transport. The final morphology shows the

ESURFD
3, 129–171, 2015

former presence of these various processes. In the three most developed valleys, the upstream end had a steeper slope than the downstream sections with a clear knickpoint separating the two (Fig. 5a). This corresponded to mudflow and fluvial flow dominating in these areas, respectively.

The collapse of unsaturated material at the valley heads resulted in steep head walls (Fig. 4). The step-wise increase of valley width and length shows this cyclic behavior (Fig. 6a and b) and results in peaks in the estimated instantaneous erosion rates (Fig. 6d). Steps in width and depth of the valleys are not simultaneous, which shows that collapse of the head- and side-walls occur at different moments. Although erosion takes place in distinct peaks of activity, the distally-fed valleys show a linear trend in valley length and width during most part of their development. Not only the length and width ratio of a single valley remain the same, but this ratio is the same for the three main valleys (Fig. 7a).

3.2 Effect of initial morphology on Distal experiment

We studied the effect of an initial morphology on the valley development in experiment Distal-after-Local by repeating the experiment on an initial morphology. This initial morphology was the result of experiment Local-2, which consists of multiple parallel shallow valleys created by overland flow (Fig. 8).

Experiment Distal-after-Local showed the same general characteristics and development as the Distal experiment. The main difference is valley initiation processes. We consider other differences as natural variations, which could have occurred without the altered initial morphology as well. In the Distal-after-Local experiment, initial seepage at the downstream end focused within the valleys of the initial morphology. However, due to groundwater flow piracy, only a limited number of these valleys fully developed. Six valleys started to form, but only two valleys fully developed (Fig. 4c). Development in the two remaining valleys was the same as described above. In the early stages of valley development, the valleys followed the path of the existing valleys in the initial morphology. When they became larger, they still followed the path of the initial valleys,

ESURFD
3, 129–171, 2015

although these were straight at this stage and the new valleys were much wider than the initial valleys. In our view, these mature valleys seemed to develop independently from the initial morphology.

3.3 Local groundwater source

The local groundwater experiment took one hour and 50 min with an average discharge of 11.9 L min^{-1}. In this experiment we distinguished two stages in valley development. In roughly the first half of the experiment, overland flow was the main source of water for valley development. In the second half, groundwater fed the valleys at their heads.

In the first stage of the experiment, the sediment in the downstream part of the slope saturated rapidly due to the limited sediment thickness (Fig. 3b-i). On this saturated sediment, precipitation transformed directly into runoff, which in turn induced valley formation by fluvial processes. These valleys started to form over the entire width of the sediment and showed valley heads with a v-shaped planform (Fig. 3b-ii). During this stage, valleys developed in headward direction by fluvial erosion and valley heads were within the area of saturated sediment. Seepage inherently occurred in the valleys due to the setup of the experiment. However, the overland flow processes dominated the seepage processes.

As the groundwater table rose during the experiment, the boundary of saturated sediment moved upslope. This progression of the saturated area slowed down as it progressed. In the first stage, valley development did not keep up with this moving front. However, the valleys caught up and developed upstream of the saturated area as the experiment progressed (Fig. 3b-iii). This marks the second stage in valley development wherein groundwater seepage rather than surface runoff fed the valley heads. From the moment the valley heads were fed by groundwater, their planform changed from v-shaped to theater-shaped (Fig. 3b-iv and b-v). This change indicates a change from fluvial flow to mass-wasting processes at the head wall. The headward growth showed similar characteristics as in the distal seepage experiment: growth governed by failure of the headwall and fluvial transport that removed the failed material. Similar

ESURFD
3, 129–171, 2015

to the distal experiments, there was also a distinguishable difference in slope in the upstream and downstream half of the valleys (Fig. 5), although this difference was less pronounced.

The valleys in the local experiment were shallow compared to the valleys in the distal experiment. In both cases, the valleys developed around the groundwater table, which was close to the surface in the local experiments. The limited depth was presumably the result of the high groundwater table, there was no zone of unsaturated sediment resulting in valleys without steep walls (Figs. 4b and 5a).

The valleys in the local experiment became longer and slightly wider by lateral erosion during the experiment (Fig. 6f and g). An important difference with the distal case was that all valleys remained active and had similar sizes during the experiment (Fig. 6i). This is due to the absence of groundwater flow piracy since each channel was fed by locally infiltrated groundwater (Fig. 4). In contrast to the distally-fed valleys, the relation between valley length and width in the locally-fed valleys is not linear and different valleys do not have the same ratio (Fig. 7b).

3.4 Effect of initial morphology on Local experiment

In the Local-after-Distal experiment, we studied the effect of the initial morphology in the opposite way as in the Distal-after-Local experiment; the final morphology of Distal acted as the initial morphology of this run (Fig. 4a). The same processes acted in this experiment, though the initial morphology had a much larger effect on the final morphology in this case.

In the first stage of the Local-after-Distal experiment, the present valleys reactivated as the sediment saturated. Due to the rising groundwater level, the steep side- and headwalls of the previous valleys became instable and collapsed. This resulted in a decreasing valley depth and increasing width. The valleys that were abandoned in the Distal experiment due to groundwater piracy reactivated as they were fed by local groundwater, resulting in a smaller difference in valley size (Fig. 4d), compared to the initial situation (Fig. 4a). Collapse of the head-wall caused headward erosion and lat-

ESURFD
3, 129–171, 2015

eral erosion caused widening of the valleys. These are the same processes as in the Local run with no initial morphology, but the final morphology showed much wider valleys. The initially present valleys were relatively deep in comparison to the final valleys. The reduction in depth of these valleys corresponded with this widening. At the end of the Local-after-Distal experiment, a body of ponding water at the flat area upstream of the valleys was released in the central valley. This resulted in the development of a feather-shaped drainage network upstream of the valley head (Fig. 4d). We do not further consider this event in this paper, but a similar morphological feature develops after the overflow of a shallow lake as result from pressurized groundwater outflow, which is discussed in Marra et al. (2014c).

4 Examples of Martian valley systems

In this section, we show the morphology of Louros Valles and Nirgal Vallis (Figs. 9 and 10), two Martian valley systems that were previously attributed to a groundwater seepage origin (e.g. Jaumann and Reiss, 2002; Harrison and Grimm, 2005; Glines and Fassett, 2013).

4.1 Louros Valles

Louros Valles are located at the north and south flanks of Valles Marineris. These valleys have circular valley heads cutting into flat plains. The valleys have a total relief of several kilometers and are between 10 and 100 km long (Fig. 9b and c). Upstream of the valley heads, there are no visible tributaries or depressions in the elevation data or imagery. Downstream of the valleys, in Valles Marineris, there are no clear deposits associated with these valleys. Sediment output in the experiments was constantly removed, in the Martian case slow could have removed the produced sediment. Alternatively, deposits could be spread over a large area on the floor of Ius Chasma as a thin veneer layer and not recognizable as fluvial deposits. The valleys on the northern flank

ESURFD
3, 129–171, 2015

are shorter than the valleys at the south. Of the southern valleys, there are two larger valleys in the west; all other valleys are approximately equal in size. The valleys are closely spaced and several valleys touch or intersect, resulting in a relatively densely dissected plain (Fig. 9c and d).

As an example, we show an elevation profile of the largest valley of Louros Valles (Fig. 9e). These and other elevation data show a rough profile with many bumps, likely related to post-valley formation wall collapse or tectonism. At the distal end of the valley, the elevation quickly drops, which shows the onset of Valles Marineris. Based on a 10 km moving average, we show the valley has a change in slope about halfway to a lower slope than the upstream part (Fig. 9e). However, the irregular elevation data limits the interpretation of these observations.

All valleys show headward-bifurcations. For the northern valleys, the orientation of the first-order valleys varies from northwest to northeast with most valleys oriented to the north-northeast (Fig. 11). The first tributaries, or second order (Hack, 1957) valleys have a similar spread in orientation, but most valleys are oriented to the west-northwest. For the southern valleys, most first-order valleys are oriented towards the southwest while higher-order valleys are directed towards the south-southwest or towards the west-southwest (Fig. 11b). Interestingly, a few third- and fourth-order segments are oriented in opposite direction (180°) as the first-order valleys (e.g. Fig. 9d).

The lengths of the tributaries range between 5 and 15 km (the main valleys are longer, but most are outside the graph), with no specific trend in the distribution of valley length (Fig. 11d). Mean bifurcation angles of the different stream-orders are between 70 and 90° (Fig. 11f).

4.2 Nirgal Vallis

Nirgal Vallis consists of one more than 500 km long main valley and several sparsely distributed side valleys of various sizes (Fig. 10). Valley depths range from several tens to several hundreds of meters. The valley cuts into the plateau through several north-to-

ESURFD
3, 129–171, 2015

south oriented wrinkle ridges, which are in places the highest points in the landscape. Several side-valleys align with these wrinkle ridges (Glines and Fassett, 2013).

The orientation of the main valley is dominantly west-northwest, the first-order tributaries have the same dominant orientation, but a large part is deflected north- and southward (Fig. 11c). This tendency of dominantly westward-oriented channels is shown in the landscape (Figs. 10d and 11c). There a few larger side valleys, but most side-valleys are very short (Figs. 10d and 11e). This results in the sparsely dissected landscape. The mean bifurcation angle between valleys is 70.7° with a standard deviation of 18.6 (Fig. 11g), similar but slightly less than the results of Glines and Fassett (2013) for the same valley network but with less measured junctions. Bifurcation angles are similar for different stream orders.

5 Discussion

5.1 Valley morphology related to source character

In this paper, we aim to find morphological properties related to different sources of groundwater in the formation of valleys by groundwater seepage. The general morphology of our experimental valleys agrees well with previous studies on sapping valleys (e.g. Howard and McLane, 1988; Hagerty, 1991; Dunne, 1980; Fox et al., 2006; Pornprommin et al., 2010). These valleys consist of half-round, theater-shaped, valley heads with a sharp transition to the upstream, uneroded surface. They develop in headward direction by destabilization of the channel head, which results from undercutting or slumping. The eroded material is transported though the valley by fluvial processes. Furthermore, in both experiments, the slope in the upstream section of the valley floor is steeper than in the downstream end (Fig. 5), which results from the transition of hyper-concentrated flow with high sediment availability at the channel heads to regular fluvial flow further downstream.

ESURFD
3, 129–171, 2015

The morphological similarity between theater-headed valleys in groundwater sapping features at the beach (Higgins, 1982), sandbox experiments (Howard and McLane, 1988), the Colorado plateau (Laity and Malin, 1985) and valleys on Mars is often used as an argument for a groundwater origin of the Martian valleys (e.g. Schumm and Phillips, 1986; Mangold and Ansan, 2006; Harrison et al., 2013). A complication in the study of such morphology on Mars is that different processes yield a similar morphology, for example waterfall erosion (Lamb et al., 2006) or groundwater weathering (Pelletier and Baker, 2011). We do not solve that in this paper since the experiments here do not explore the morphological difference between different processes. Here, we focus on groundwater processes in further detail.

In the following discussion, we propose different end-member landscapes based on knowledge from our experiments combined with previous experimental and modeling results and theoretical considerations. The main landscape properties are the distribution of valley lengths, valley order, valley spacing and bifurcations. We interpret the Martian valleys described above in this framework and end with considerations on the applicability of scaled experiments of such systems.

5.2 Scalability of experimental results

An important difference between the distal and local groundwater experiments was the steepness of the valley heads and sidewalls, which were much steeper in the distal groundwater case. In the Distal experiment, the groundwater table was deeper, resulting in an unsaturated (moist) top layer above the groundwater table, which has more apparent cohesion than the saturated (wet) top layer in the locally infiltrated groundwater case. In natural systems, such properties show differences in soil properties rather than formative processes. The depth of the unsaturated layer relates to capillary forces, which are scale-independent and thus relatively small for large experimental valleys (see discussion in Marra et al., 2014a). Nevertheless, theater head formation took place in both cases with and without an unsaturated top-layer, which indicates that this process takes place under both conditions and is not the result of this scale-effect.

ESURFD
3, 129–171, 2015

Destabilization of the headwall is a necessary condition for the development of sapping valleys. This only takes place if sufficient sediment is removed from the toe of the headwall, which requires enough discharge for sediment transport. In previous smaller sapping experiments (Marra et al., 2014a), there were problems with sustaining the process without artificial removal of sediment. In our current experiment, the discharge was sufficient to allow continuous downstream sediment transport. Marra et al. (2014a) report on experiments in a 1 × 3 m setup with sand where the valleys clogged due to the absence of downstream sediment removal (these are not the main experiments reported in that paper, they are mentioned in the discussion). Their solution to keep the upstream processes and valley formation going was to flush away sediment at the downstream end. In that same setup, sapping valleys did develop when lightweight plastic sediment was used, resulting in sufficient sediment transport. Similarly, the larger experiment by Howard and McLane (1988) featured a downstream gutter to remove the sediment and maintain the process of sediment evacuation from the growing valley. In the experiments described in this study, sediment was not flushed at the downstream end and the downstream elevation is kept constant by a row of bricks. In other words, the processes that occurred were not forced by the removal of downstream sediment, which shows that the scale-effect of having a too low discharge for sediment was overcome in our setup.

5.3 Groundwater piracy, valley spacing and length distribution

The morphology of the entire landscape shows important differences that are related to subsurface processes. In the distally-fed experiment, a decreasing number of channels remained active when small valleys ceased to develop. This behavior is related to groundwater piracy of the larger valleys and results in an increase of valley spacing. The valleys are depressions and therefore attract groundwater. Due to the travel distance and direction of the groundwater, areas downstream of large valleys receive less groundwater. The resulting landscape consists of a few large and several small valleys in between, which ceased developing due to this cutoff of groundwater (Fig. 4a),

ESURFD
3, 129–171, 2015

and valleys are mainly oriented towards the groundwater source (Fig. 12a). In contrast, the locally-fed channels did not feature groundwater flow piracy, which results in a densely dissected landscape with valleys of similar size in close proximity of each other (Figs. 4b and 12b). The close proximity is a strong indication that the availability of water was not limiting and piracy can therefore not have been important.

An important parameter for flow piracy is the fraction of the groundwater flow that a valley captures. This is controlled by the fraction of cross-stream to downstream groundwater flux (Pelletier, 2003; Schorghofer et al., 2004), which is proportional to the groundwater gradient in isotropic conditions. In the case of sapping valleys, the emerging valley itself leads to a topographic low that introduces a cross-stream groundwater slope, which increases the flow towards that valley. This morphological feedback causes flow piracy when a valley attracts enough flow to cease the development of another valley. This feedback and tendency for flow piracy, is stronger for lower regional slopes as a perturbation has a relative large effect on the groundwater flow (Pornprommin et al., 2010).

Our experiments show that the valley width-to-length ratio is similar for valleys formed by a distal source of groundwater (Fig. 7a), which was not the case for the locally-fed valleys (Fig. 7a). Such similarity in the development of several distally-fed valleys is indicative for valley formation by the same source of groundwater. The size of the valleys dominantly control the amount of water delivered to that valley since a larger valley source yields more seepage. In turn, the amount of erosion relates to the size of the valley and hence, the morphological development is similar for the different valleys. The amount of water delivered to the locally-fed channels is only partly controlled by this mechanism. In this case, the amount of groundwater delivered to the valley head also depends on upstream area and local watersheds.

Initial conditions may affect the location and thus spacing of valleys. In our distally-fed experiment with minor initial morphology (Distal-after-Local), the initiation of sapping valleys seemed related to the initial perturbation, but the resulting processes and landscape was similar to the experiment with no initial perturbations. This shows that

ESURFD
3, 129–171, 2015

seepage is robustly driven by the subsurface flow pattern and agrees with the observations of Schumm and Phillips (1986): valleys of a composite origin dominantly reflect the last process. In contrast, in the locally-fed experiment with initial perturbations (Local-after-Distal), there was a major effect as old valleys reactivated and dominated the final morphology.

The strong difference of local effects is the result of the groundwater flow patterns: in the locally-fed experiments, local perturbations affect the flow pattern, while groundwater from a distal source is driven dominantly by the large-scale morphology. Furthermore, flow piracy dampens the development of small perturbations. An important implication is that the location and orientation of distally-fed sapping valleys strongly relate to the hydrological system and can thus be used as an indicator of the possible source of groundwater.

5.4 Headward channel bifurcations

Our experimental valleys did not bifurcate at their channel head, which is considered a typical property for sapping valleys (e.g. Howard and McLane, 1988). The absence of bifurcations in our experiments is the result of the steep slope in the downstream half of the setup. Pornprommin et al. (2010) showed that a low regional slope, and thus lower morphological feedback, resulted in more seepage at the flanks of the valley head, which increased the tendency of the valleys to bifurcate. Our results show that seepage on a relatively steep slope suppresses the tendency to form bifurcations, compared with similar experiments with a horizontal surface, which do show bifurcations (Fig. 12a and c; e.g. Berhanu et al., 2012).

Besides the regional slope, Berhanu et al. (2012) showed that valleys fed from a local source have a higher tendency to bifurcate in headward direction. This tendency relates to the groundwater flow that enters the channel head from a wide range of directions and not mainly from upstream of the valley. The typical flow field that results from local infiltration in a flat substrate results in bifurcations with a typical angle of 72° (Devauchelle et al., 2012). In such system, the valleys would have many bi-

ESURFD
3, 129–171, 2015

furcations which results in a densely dissected landscape (Fig. 12d), similar to the Apalachicola Bluffs (Florida) which were formed by seepage of locally infiltrated precipitation (Abrams et al., 2009). The valleys in this system could be subject to flow piracy, but as a result by other valleys cutting each other off. This mechanism of piracy is different from the piracy by groundwater flow capture, which acts on a larger distance and is typical for distally-fed valleys.

The combined occurrence of developing bifurcations and groundwater piracy results in the formation of typically stubby tributaries. When a valley bifurcates, there are two channel heads close to each other, which will in many cases result in abandonment of one of the two (Fig. 12c). This behavior and resulting morphology is indicative of sapping from a distal groundwater source.

5.5 Origin of Martian examples

In this paper, we analyzed the landscape of Louros and Nirgal Vallis, two valley systems often attributed to groundwater seepage. Two additional examples are shown in Fig. 12a and b. The valleys in Noctis Labyrinthus (Fig. 12a) show valleys with no bifurcations and a few small valleys in between larger valleys. Although the plateau where these valleys cut into is flat, there is a strong gradient between valley head and outflow point, which is what we mean with a steep slope and which is what suppresses the tendency to bifurcate. The small valleys in Gale Crater (Fig. 12b) are similar in size, shallow and the there is a regional slope. These examples serve as an illustration on how the morphology can appear, but are not further analyzed here.

Alternate hypotheses for similar valley formation are bedrock erosion by catastrophic release of surface water (Lamb et al., 2006) or bedrock weathering rather by groundwater (Pelletier and Baker, 2011). The latter would yield a similar morphology as sapping in unconsolidated material, and the two processes would likely act in the same systems as the weathered bedrock material is further removed by seeping groundwater. However, weathering in bedrock could result in steep slopes, which are not likely for large valleys in case of seepage erosion in unconsolidated material (Marra et al., 2014a).

ESURFD
3, 129–171, 2015

The evidence in favor of a groundwater origin on both cases is the absence of upstream feeder channels to the main valleys. However, billions of years of weathering and a dust cover could have obscured such channels. The elevation profile of one of the Louros Valles is bumpy, likely due to later activity. Based on filtered elevation profile, the valley shows a lower slope downstream, similar to the experiments, but the implication of this is limited due to the bumpiness of the profile.

The orientation of valley segments of Louros Valles is diverse with wide bifurcation angles and a broad range of valley lengths, resulting in a densely dissected landscape (Fig. 9). Such landscape is typical for a local groundwater source (Fig. 12d). The bifurcation angles have a much broader distribution than the theoretical value for such system. This could be the effect of valleys aligning with the tectonic structure, which would result in 90° angles (Luo et al., 1997). Furthermore, in Louros Valles, some higher-order valley segments are oriented in opposite direction of the main valleys, which can only be explained by a local source of groundwater and not by surface flow following the topography.

A possible source of groundwater for Louros Valles is precipitation; melt of snow, ice or permafrost; or upwelling groundwater from a cryosphere-confined aquifer. Another source of water could be vertical upwelling groundwater from an aquifer. Such aquifer in this region may relate to the outflow channels further northeast, although the timing of events here is crucial. The presence of Valles Marineris, and the clear formation of Louros Valles after the opening of Valles Marineris, suggest that this aquifer was at that point cut-off, and in fact split between north and south. Seepage at Louros Valles rather than the formation of an outflow channel could represent a low aquifer pressure, which fits a trend of lower groundwater pressures at higher elevations in Ophir and Lunae Plana (Marra et al., 2014b). An alternate hypothesis for the formation of Louros Valles is by focussed erosion of meltwater in between patches protected from erosion by the presence of an ice-cover ("glacial selective linear erosion", Lee, 2000).

Nirgal Vallis cuts through some ridges in the landscape where surface runoff would have flowed around. If this landscape is indeed formed by groundwater, the source is

ESURFD
3, 129–171, 2015

likely distal, given the large number of small valleys typical for groundwater piracy due to a distal source (Figs. 10, 4a, 12a and c). The source was likely west of the valley due to the orientation of most valleys towards that direction. The average bifurcation angle is close to 72°, which is considered a typical angle for groundwater-seepage valleys and mentioned as evidence for a groundwater origin by Glines and Fassett (2013). However, this value is only valid for valleys formed by a local source of groundwater (Devauchelle et al., 2011), which is not the case here, and such value is heavily influenced by subsurface conditions like tectonic structures (e.g. Luo et al., 1997).

A possible source of groundwater for Nirgal Vallis is groundwater flow from the west, which is ultimately recharged from Tharsis. Seepage of groundwater could have taken place before the formation of a confining cryosphere. Alternatively, if the cryosphere was already present, discontinuities or rupture could have triggered outflow from a confined aquifer. However, in this case the groundwater should have flown laterally first to account for the morphology, which would be the case if the groundwater pressure was not sufficient to induce artesian seepage. Seepage would then occur further downstream at topographic depressions.

Based on our and previous experiments, this study now provides a framework which links the landscape to the groundwater source characteristics. The two Martian examples shown further illustrate this link. Although different processes could produce similar valley morphologies, the strong correspondence of the landscape metrics of these examples and those produced by sapping hints at a groundwater origin. Particularly the distant groundwater source of Nirgal Vallis implies a well-developed groundwater system. Perhaps most significantly, outflow and valley formation of such system could have taken place regardless of climate conditions optimal for sustained presence of liquid water on the surface.

ESURFD
3, 129–171, 2015

6 Conclusions

We studied groundwater seepage processes and subsequent valley formation using large sandbox experiments. Our experiments focused on the difference between locally- or distally-fed valleys on a steep slope. In both cases, valley heads developed in headward direction by mass-wasting processes triggered by steepening due to fluvial sediment transport out of the valley.

Combined with previous experimental work, we provide a framework of driving processes and resulting landscape metrics for sapping valleys fed by a distal and local source, and for steep and flat topography. Their main characteristics are as follows. (1) Due to groundwater piracy, seepage erosion from a distant groundwater source results in a sparsely dissected landscape with a few large and many small valleys. Valleys fed by a local groundwater source, for example infiltrating precipitation or melt of ground ice, are not characterized by flow piracy and have a range sizes, resulting in a densely dissected landscape. (2) Valley formation in horizontal surfaces promote the development of bifurcations in contrast to steep surfaces where this tendency is suppressed. For distally-fed sapping, the combined occurrence of bifurcating valleys and flow piracy results in valley systems with stubby tributaries. Locally-fed sapping valleys on horizontal surfaces grow in a wide range of directions due to the occurrence and prevalence of bifurcations.

As an example, we applied these characteristics to two Martian systems. Firstly, Louros Valles shows a densely dissected landscape with a broad range of valley orientations and valley lengths. This landscape is typical for a local groundwater source. Such local source could relate to an aquifer that fed the outflow channels, but is more likely related to local precipitation or melt of ice or snow. Secondly, Nirgal Vallis whos a sparely dissected landscape with many small and only a few large valleys that are oriented dominantly to the west. This indicates a distal groundwater source in the west, which is likely produced from recharge at Tharsis. Further study of similar landscape

ESURFD
3, 129–171, 2015

properties as result of overland flow is required to further resolve the ambiguous interpretation of these valleys.

The Supplement related to this article is available online at doi:10.5194/-15-129-2015-supplement.

Author contributions. Study conception: W. A. Marra, E. Hauber, M. G. Kleinhans; Experimental design: W. A. Marra, S. J. McLelland, B. J. Murphy, D. R. Parsons, M. G. Kleinhans; Analyses and interpretation: W. A. Marra; Discussion of the results: W. A. Marra, E. Hauber and M. G. Kleinhans with contribution from all other authors; W. A. Marra wrote the paper.

Acknowledgements. This work is part of the PhD research of W. A. Marra, financially supported by NWO grant ALW-GO-PL/10 01. The authors are grateful for the time-lapse camera triggering device build by Henk Markies, for the help by Tjalling de Haas, Steven de Jong, Leiping Ye, Chris Unsworth, Susan Conway and Rob Thomas in running the experiments and Tjalling de Haas for reviewing a draft of this paper. Experimental data are available upon request from W. A. Marra (w.a.marra@uu.nl) or M. G. Kleinhans (m.g.kleinhans@uu.nl).

References

Abrams, D. M., Lobkovsky, A. E., Petroff, A. P., Straub, K. M., McElroy, B., Mohrig, D. C., Kudrolli, A., and Rothman, D. H.: Growth laws for channel networks incised by groundwater flow, Nat. Geosci., 2, 193–196, doi:10.1038/ngeo432, 2009. 132, 150

Agisoft: Agisoft PhotoScan User Manual: Professional Edition, Version 1.0, available at: http://www.agisoft.com/, 2014. 136

Berhanu, M., Petroff, A., Devauchelle, O., Kudrolli, A., and Rothman, D. H.: Shape and dynamics of seepage erosion in a horizontal granular bed, Phys. Rev. E, 86, 041304-1–041304-9, doi:10.1103/PhysRevE.86.041304, 2012. 132, 149

Craddock, R. A., Howard, A. D., Irwin, R. P., Tooth, S., Williams, R. M. E., and Chu, P.-S.: Drainage network development in the Keanakāko'i tephra, Kīlauea Volcano, Hawai'i: implica-

ESURFD
3, 129–171, 2015

tions for fluvial erosion and valley network formation on early Mars, J. Geophys. Res., 117, 1–19, doi:10.1029/2012JE004074, 2012. 131
Devauchelle, O., Petroff, A. P., Lobkovsky, A. E., and Rothman, D. H.: Longitudinal profile of channels cut by springs, J. Fluid Mech., 667, 38–47, doi:10.1017/S0022112010005264, 2011. 152
Devauchelle, O., Petroff, A. P., Seybold, H. F., and Rothman, D. H.: Ramification of stream networks., P. Natl. Acad. Sci. USA, 109, 20832–20836, doi:10.1073/pnas.1215218109, 2012. 132, 149
Dunne, T.: Formation and controls of channel networks, Prog. Phys. Geog., 4, 211–239, doi:10.1177/030913338000400204, 1980. 145
Fergason, R., Lee, E. M., and Weller, L.: Themis geodetically controlled mosiacs of Mars, Lunar Planet. Sci. Conf., XLIV, abstract 1642, The Woodlands, Texas, 18–22 March, 2013. 137
Forsyth, D. A. and Ponce, J.: Computer Vision: a Modern Approach, 2nd Edn., Prentice Hall, Upper Saddle River, New Jersey, 2011. 135
Fox, G. A. and Wilson, G. V.: The role of subsurface flow in hillslope and stream bank erosion: a review, Soil Sci. Soc. Am. J., 74, 717–733, doi:10.2136/sssaj2009.0319, 2010. 131
Fox, G. A., Wilson, G. V., Periketi, R. K., and Cullum, R. F.: Sediment transport model for seepage erosion of streambank sediment, J. Hydraul. Eng.-ASCE, 11, 603–611, doi:10.1061/(ASCE)1084-0699(2006)11:6(603), 2006. 145
Glines, N. and Fassett, C. I.: Evidence for Groundwater Sapping on Mars from Junction Angles of Nirgal Vallis Tributaries, in: Lunar Planet. Sci. Conf., Vol. XLIV, p. abstract 2011, The Woodlands, Texas, 18–22 March, 2013. 132, 138, 143, 145, 152
Hack, J. T.: Studies of Longitudinal Stream Profiles in Virginia and Maryland, US Geol. Suvey Prof. Pap., 294-B, Washington D.C., 1957. 137, 144
Hagerty, D. J.: Piping/sapping erosion. I: Basic considerations, J. Hydraul. Eng.-ASCE, 117, 991–1008, doi:10.1061/(ASCE)0733-9429(1991)117:8(991), 1991. 131, 145
Harrison, K. P. and Grimm, R. E.: Groundwater-controlled valley networks and the decline of surface runoff on early Mars, J. Geophys. Res., 110, E12S16, doi:10.1029/2005JE002455, 2005. 130, 143
Harrison, S., Balme, M., Hagermann, A., Murray, J., Muller, J.-P., and Wilson, A.: A branching, positive relief network in the middle member of the Medusae Fossae Formation, equatorial Mars-Evidence for sapping?, Planet. Space Sci., 85, 142–163, doi:10.1016/j.pss.2013.06.004, 2013. 146

ESURFD
3, 129–171, 2015

Higgins, C. G.: Drainage systems developed by sapping on Earth and Mars, Geology, 10, 147–152, doi:10.1130/0091-7613(1982)10<147:DSDBSO>2.0.CO;2, 1982. 131, 146

Howard, A. D. and Kochel, R. C.: Introduction to Cuesta landforms and sapping processes on the Colorado Plateau, in: Sapping Featur. Color. Plateau, edited by: Howard, A. D., Kochel, R. C., and Holt, H. R., chap. 2, 6–56, NASA Spec. Publ. 491, Washington D.C., 1988. 131

Howard, A. D. and McLane, C. F.: Erosion of cohesionless sediment by groundwater seepage, Water Resour. Res., 24, 1659–1674, doi:10.1029/WR024i010p01659, 1988. 131, 132, 145, 146, 147, 149

Irwin, R. P., Tooth, S., Craddock, R. A., Howard, A. D., and de Latour, A. B.: Origin and development of theater-headed valleys in the Atacama Desert, northern Chile: morphological analogs to Martian valley networks, Icarus, 243, 296–310, doi:10.1016/j.icarus.2014.08.012, 2014. 131

Jaumann, R. and Reiss, D.: Nirgal Vallis: evidence for Extensive Sapping, in: Lunar Planet. Sci. Conf., p. abstract 1579, The Woodlands, Texas, 11–15 March, 2002. 132, 138, 143

Jaumann, R., Neukum, G., Behnke, T., Duxbury, T., Eichentopf, K., Flohrer, J., Gasselt, S., Giese, B., Gwinner, K., Hauber, E., Hoffmann, H., Hoffmeister, a., Köhler, U., Matz, K.-D., McCord, T., Mertens, V., Oberst, J., Pischel, R., Reiss, D., Ress, E., Roatsch, T., Saiger, P., Scholten, F., Schwarz, G., Stephan, K., and Wählisch, M.: The high-resolution stereo camera (HRSC) experiment on Mars Express: instrument aspects and experiment conduct from interplanetary cruise through the nominal mission, Planet. Space Sci., 55, 928–952, doi:10.1016/j.pss.2006.12.003, 2007. 137

Kochel, R. C. and Piper, J. F.: Morphology of large valleys on Hawaii: evidence for groundwater sapping and comparisons with Martian valleys, J. Geophys. Res., 91, E175, doi:10.1029/JB091iB13p0E175, 1986. 131

Laity, J. E. and Malin, M. C.: Sapping processes and the development of theater-headed valley networks on the Colorado Plateau, Geol. Soc. Am. Bull., 96, 203–217, doi:10.1130/0016-7606(1985)96%3C203:SPATDO%3E2.0.CO;2, 1985. 131, 146

Lamb, M. P., Howard, A. D., Johnson, J., Whipple, K. X., Dietrich, W. E., and Perron, J. T.: Can springs cut canyons into rock, J. Geophys. Res., 111, 7002, doi:10.1029/2005JE002663, 2006. 131, 146, 150

ESURFD
3, 129–171, 2015

Lee, P.: Selective fluvial erosion on mars: glacial selective linear erosion on Devon island, Nunavut, arctic Canada, as a possible analog, Lunar Planet. Sci. Conf., XXXI, abstract 2080, The Woodlands, Texas, 13–17 March, 2000. 151

Lobkovsky, A. E., Jensen, B., Kudrolli, A., and Rothman, D. H.: Threshold phenomena in erosion driven by subsurface flow, J. Geophys. Res., 109, 1–10, doi:10.1029/2004JF000172, 2004. 132

Luo, W., Arvidson, R. E., Sultan, M., Becker, R., Katherine Crombie, M., Sturchio, N., and El Alfy, Z.: Ground-water sapping processes, Western Desert, Egypt, Geol. Soc. Am. Bull., 109, 43–62, doi:10.1130/0016-7606(1997)109<0043:GWSPWD>2.3.CO;2, 1997. 151, 152

Mangold, N. and Ansan, V.: Detailed study of an hydrological system of valleys, a delta and lakes in the Southwest Thaumasia region, Mars, Icarus, 180, 75–87, doi:10.1016/j.icarus.2005.08.017, 2006. 146

Marra, W. A., Braat, L., Baar, A. W., and Kleinhans, M. G.: Valley formation by groundwater seepage, pressurized groundwater outbursts and crater-lake overflow in flume experiments with implications for Mars, Icarus, 232, 97–117, doi:10.1016/j.icarus.2013.12.026, 2014a. 132, 146, 147, 150

Marra, W. A., Hauber, E., de Jong, S. M., and Kleinhans, M. G.: Pressurized groundwater systems in Lunae and Ophir Plana (Mars): insights from small-scale morphology and experiments, submitted, 2014b. 151

Marra, W. A., Hauber, E., McLelland, S. J., Murphy, B. J., Parsons, D. R., Conway, S. J., Roda, M., Govers, R., and Kleinhans, M. G.: Pressurized groundwater outflow experiments and numerical modeling for outflow channels on Mars, J. Geophys. Res.-Planet., 119, 2668–2693, doi:10.1002/2014JE004701, 2014c. 143

Marra, W. A., Kleinhans, M. G., and Addink, E. A.: Network concepts to describe channel importance and change in multichannel systems: test results for the Jamuna River, Bangladesh, Earth Surf. Proc. Land., 39, 766–778, doi:10.1002/esp.3482, 2014d. 137

Otvos, E. G.: Rain-induced beach processes; landforms of ground water sapping and surface runoff, J. Coastal Res., 15, 1040–1054, 1999. 131

Pelletier, J. D.: Drainage basin evolution in the Rainfall Erosion Facility: dependence on initial conditions, Geomorphology, 53, 183–196, doi:10.1016/S0169-555X(02)00353-7, 2003. 148

Pelletier, J. D. and Baker, V. R.: The role of weathering in the formation of bedrock valleys on Earth and Mars: a numerical modeling investigation, J. Geophys. Res., 116, 1–13, doi:10.1029/2011JE003821, 2011. 146, 150

ESURFD
3, 129–171, 2015

Pornprommin, A., Takei, Y., Wubneh, A. M., and Izumi, N.: Channel inception in cohesionless sediment by seepage erosion, J. Hydro-Env. Res., 3, 232–238, doi:10.1016/j.jher.2009.10.011, 2010. 132, 139, 145, 148, 149

Schorghofer, N., Jensen, B., Kudrolli, A., and Rothman, D. H.: Spontaneous channelization in permeable ground: theory, experiment, and observation, J. Fluid Mech., 503, 357–374, doi:10.1017/S0022112004007931, 2004. 132, 148

Schumm, S. A. and Phillips, L.: Composite channels of the Canterbury Plain, New Zealand: a Martian analog?, Geology, 14, 326, doi:10.1130/0091-7613(1986)14<326:CCOTCP>2.0.CO;2, 1986. 131, 146, 149

ESURFD

3, 129–171, 2015

Table 1. Experimental runs, their duration, discharge setting and data acquisition intervals, video number corresponds with videos in the Supplement.

Experiment	Duration	Mean Q ($L\,min^{-1}$)	Cumm. Q (m^3)	Time-lapse interval	SfM interval	video
Distal	3 d 3 h	2.4	10	5 min	1 d 3 h 2 d 2 h 2 d 22 h 3 d 3 h	video 1
Local	1 h 50 min	11.9	0.95	30 s	end of exp.	video 2
Local 2	40 min					
Local after Distal	3 h 10 min	10.5	1.9	30 s	end of exp.	video 3
Distal after Local	3 d 16 h	2	10	5 min	2 h 21 h 2 d 0 h 2 d 20 h 3 d 16 h	video 4

ESURFD
3, 129–171, 2015

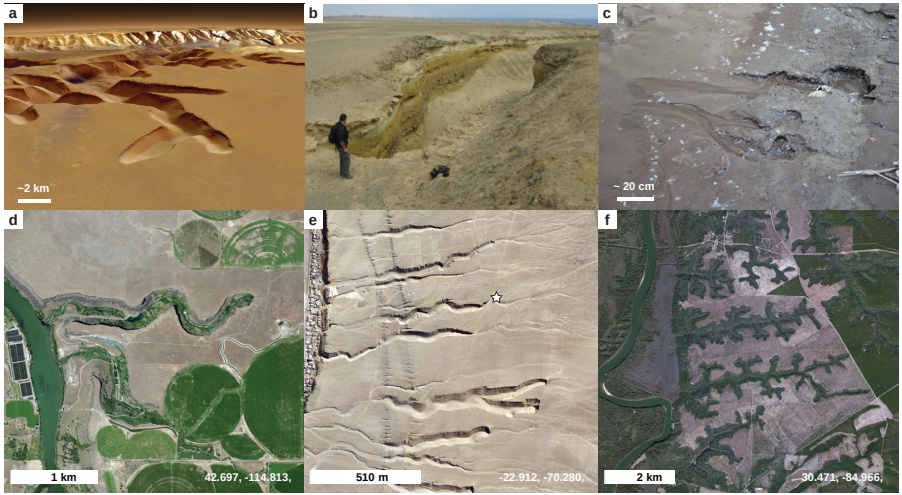

Figure 1. Examples of theater-headed valleys. **(a)** Louros Valles on Mars, (perspective view); **(b)** valleys on the coast of the Atacama Desert, Chile (oblique photo, human for scale); **(c)** a riverbank (oblique photo); **(d)** Side valleys of Snake River, Idaho, USA (orthorectified image); **(e)** valleys on the coast of the Atacama Desert, star indicates position of viewpoint of **(b)** (orthorectified image); **(f)** Apalachicola bluffs near Bristol, Florida, USA (orthorectified image). Image credits: **(a)** Google Earth (NASA/USGS, ESA/DLR/FU Berlin), **(b)** Tjalling de Haas, **(c)** Wouter Marra, **(d, f)** Bing Maps Imagery, **(d)** Courtesy of GFZ Potsdam.

ESURFD
3, 129–171, 2015

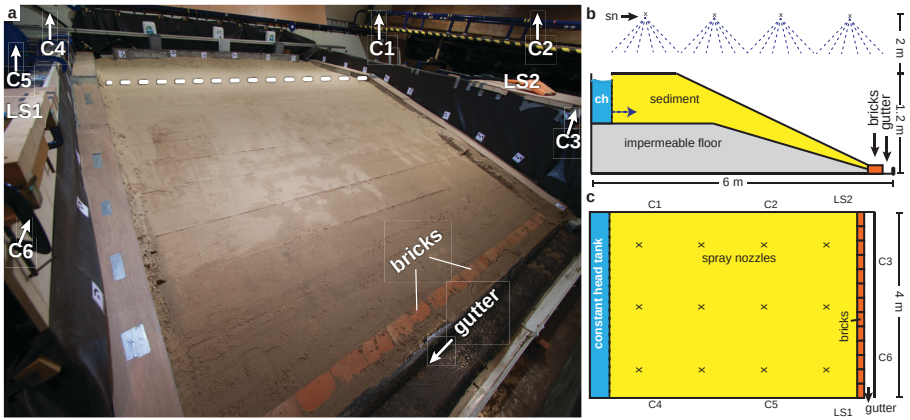

Figure 2. Setup of the sapping experiments. **(a)** Oblique photo from downstream end of the flume, showing the initial sediment surface, gutter and constant head tank in the back. The rain simulators and cameras are above the photographed area; their approximate locations (C1–C6) are shown. **(b)** Cross section showing setup with impermeable floor, constant head tank (ch), gutter, approximate location of spray nozzles (sn) and brickwork. **(c)** Plan view showing the locations of the rain simulators (x), camera locations (C1–C6) and positions of the laser scanner (LS1, LS2).

ESURFD
3, 129–171, 2015

Groundwater seepage landscape experiments

W. A. Marra et al.

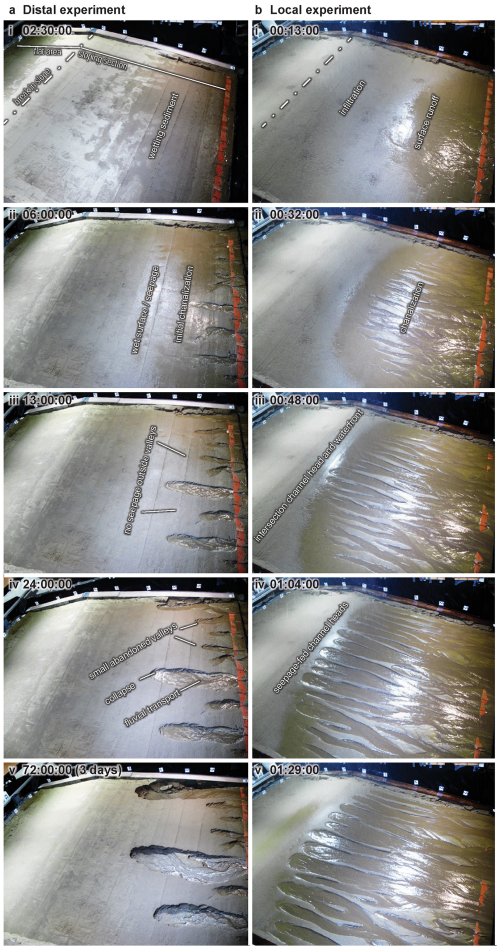

Figure 3. Stills from time-lapses of the experiments showing the main morphological development. Full time-lapse movie are available in the Supplement.

ESURFD
3, 129–171, 2015

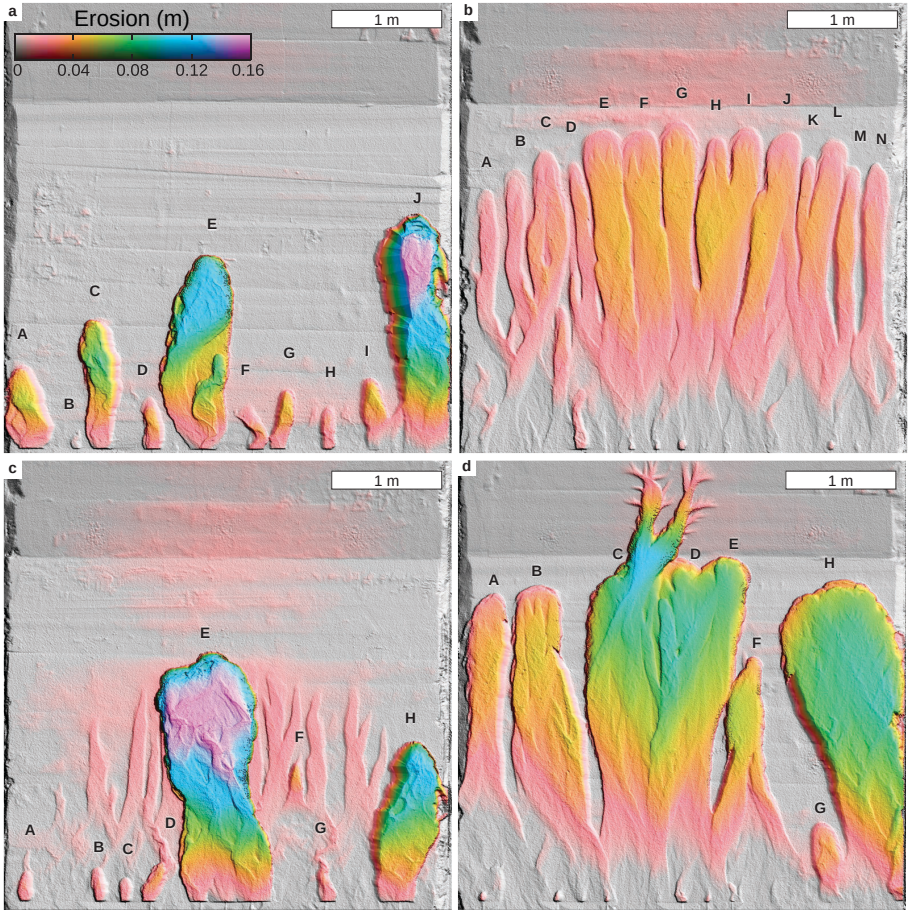

Figure 4. Erosion maps/final morphology of the experiments showing valley letters used in subsequent figures. **(a)** Distal experiment, **(b)** Local experiment **(c)** Distal after Local and **(d)** Local after Distal.

ESURFD
3, 129–171, 2015

Groundwater seepage landscape experiments

W. A. Marra et al.

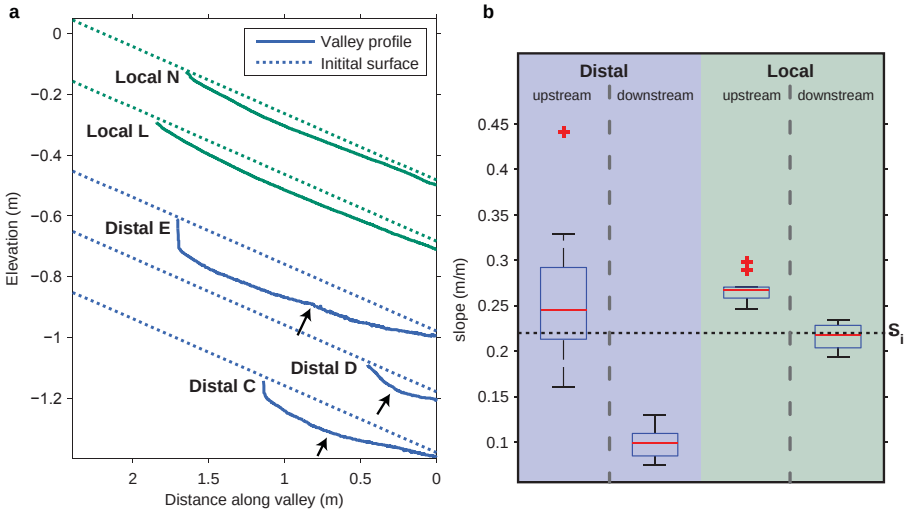

Figure 5. Channel profiles and slopes. **(a)** Channel profiles of valleys C, D and E of distal experiment and valleys N and L of local experiment, displayed with factor 2 vertical exaggeration. Elevations are arbitrary and plotted with offset for clarity. The three distal experiment profiles show three arrested stages of development also seen in larger valleys: incipient sapping valley without a steep valley head (D), developing valley with moderate steep valley head (C) and developed valley with steep valley head and reduced valley floor gradient (E), arrows indicate break in slope at the valley floow. **(b)** Boxplot of slope in upstream and downstream part of all valleys in distal (n = 9) and local (n = 14) experiments. The horizontal dotted line shows the initial surface slope S_i = 0.22.

ESURFD
3, 129–171, 2015

Groundwater seepage landscape experiments

W. A. Marra et al.

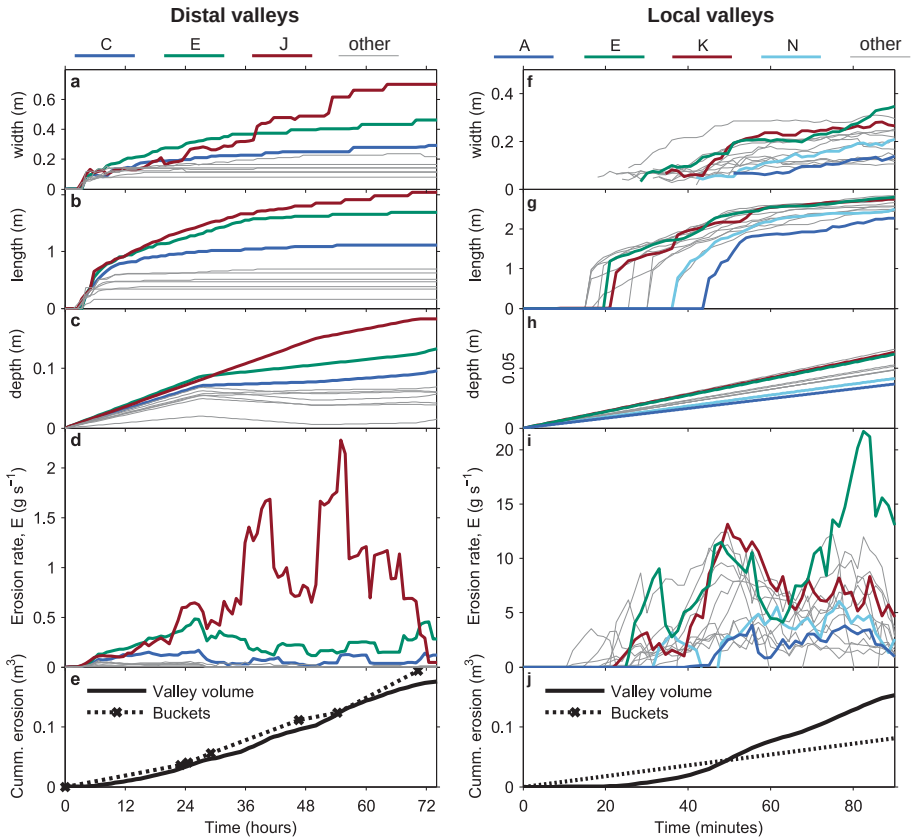

Figure 6. Valley development in the distal (left panel) and local (right panel) experiment. Main valleys indicated with colors, letters in legend correspond with letters in Fig. 4. **(a, f)** Valley width and **(b, g)** length derived from orthorectified time-lapse imagery, **(c, h)** valley depth derived from SFM-dems, **(d, i)** estimated erosion rated from these properties and **(e, j)** total cumulative erosion estimate from valley volume compared to measured sediment output.

ESURFD
3, 129–171, 2015

Groundwater seepage landscape experiments

W. A. Marra et al.

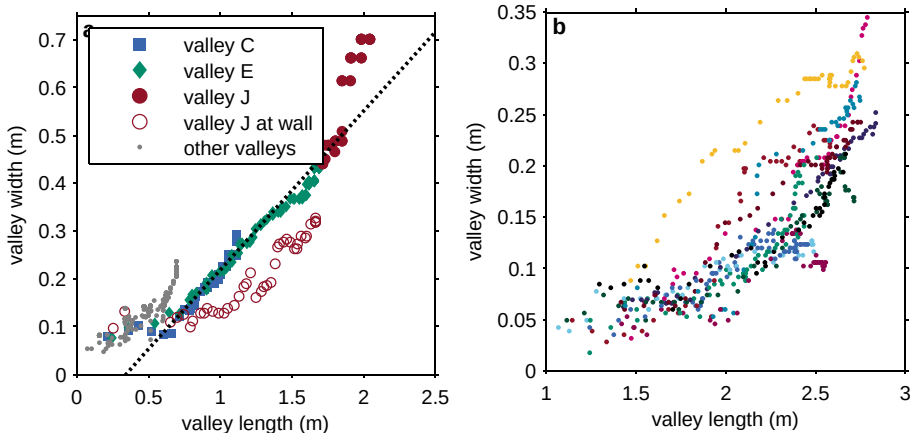

Figure 7. Development of valley width vs. length of the **(a)** distal and **(b)** local experiment. Colored symbols in panel a represent the three main valleys. Values are plotted for all time-lapse intervals (valley dimensions increase with time). The open symbols in panel a represent valley dimensions when the measured valley section flowed at the side wall which influenced the valley width. Dotted line indicates trend of the three persisting valleys when the flume wall did not influence their width.

ESURFD
3, 129–171, 2015

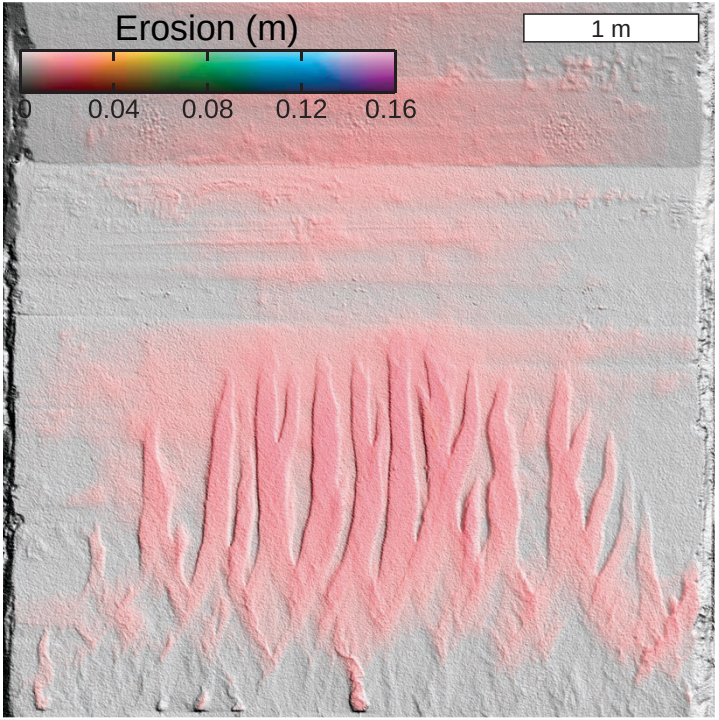

Figure 8. Final morphology of experiment Local 2, which is the initial morphology of experiment Distal after Local.

ESURFD
3, 129–171, 2015

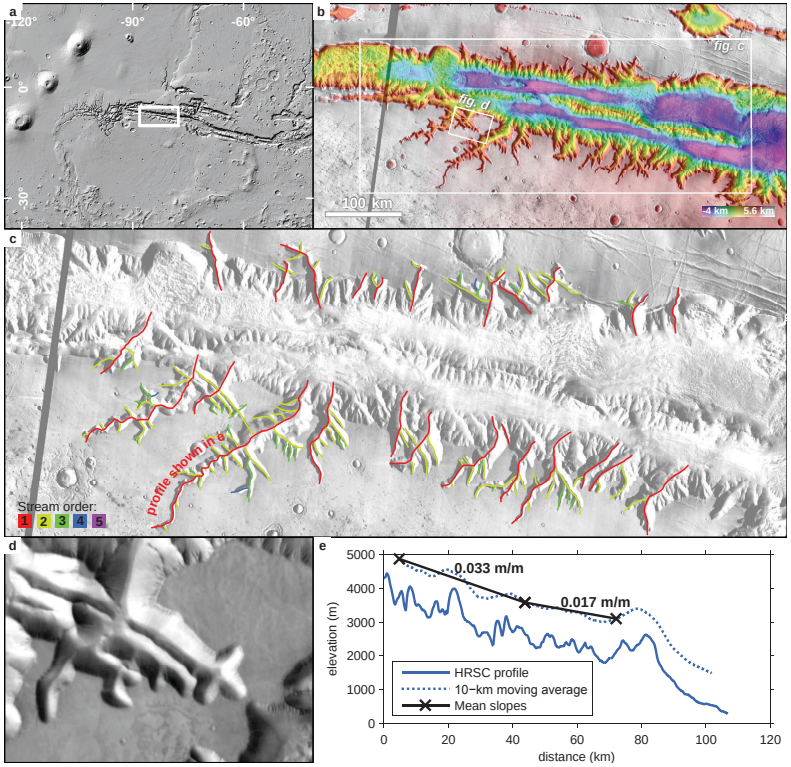

Figure 9. Maps and profile of Louros Valles. **(a)** Overview map showing location of **(b)** (MOLA shaded relief). **(b)** THEMIS daytime infrared mosaic with color-coded MOLA DEM, showing location of (**c** and **d**). **(c)** Valley centerlines, color-coded with stream-order on THEMIS day-IR mosaic. **(d)** Detail of the network showing a densely dissected landscape and bifurcating valleys. **(e)** Elevation profile based on HRSC data, moving average using a 10 km window (plotted with 1000 m vertical offset) and slopes of two segments. Location of this profile is the first order valley indicated in **(c)**.

ESURFD
3, 129–171, 2015

Groundwater seepage landscape experiments

W. A. Marra et al.

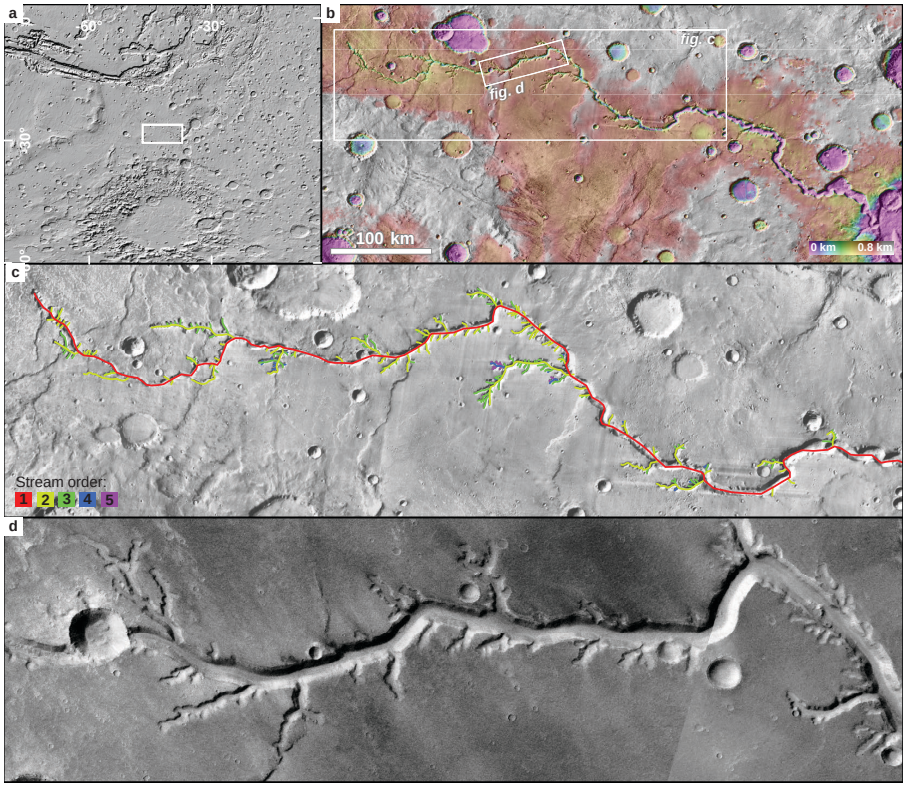

Figure 10. Maps of Nirgal Vallis. **(a)** Overview map showing location of **(b)** (MOLA shaded relief). **(b)** THEMIS daytime infrared mosaic with color-coded MOLA DEM, showing location of (**c** and **d**). **(c)** Valley centerlines, color-coded with stream-order on THEMIS day-IR mosaic. **(d)** Detail of the network showing a sparsely dissected landscape with many small and a few large valleys.

ESURFD
3, 129–171, 2015

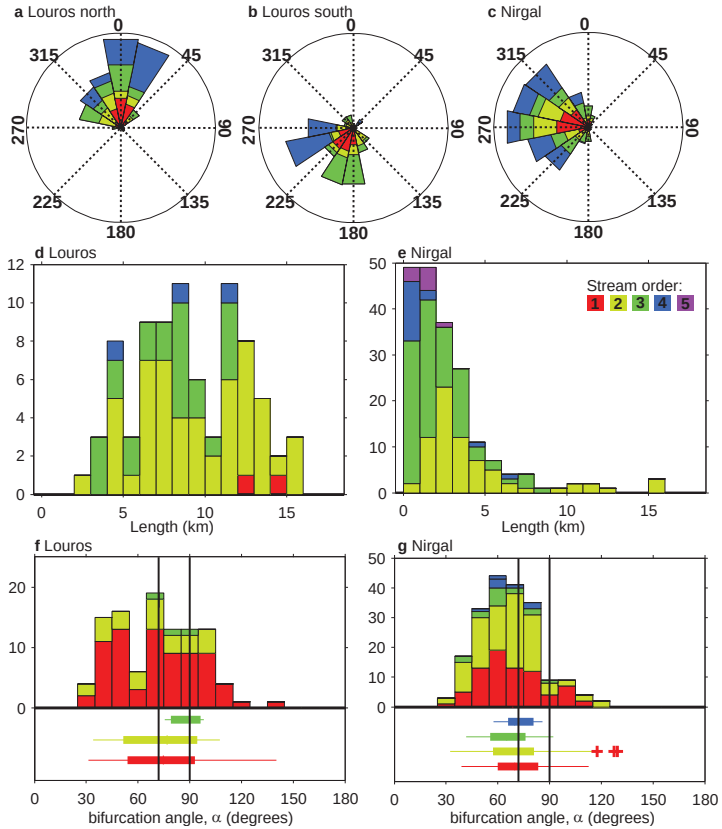

Figure 11. Landscape metrics of Louros and Nirgal Vallis. **(a–c)** Valley orientation for valleys on the north **(a)** and south flank **(d)** of Louros Valles and Nirgal Vallis **(c)**. (**d** and **e**) Valley length (distance to lower-order valley) distribution for different stream orders, most main valleys (order 1) plot far outside the shown window for **(d)** Louros and **(e)** Nirgal Vallis. (**f** and **g**) Distribution of bifurcation orientation and boxplots per stream order for **(f)** Louros and **(g)** Nirgal Vallis.

ESURFD
3, 129–171, 2015

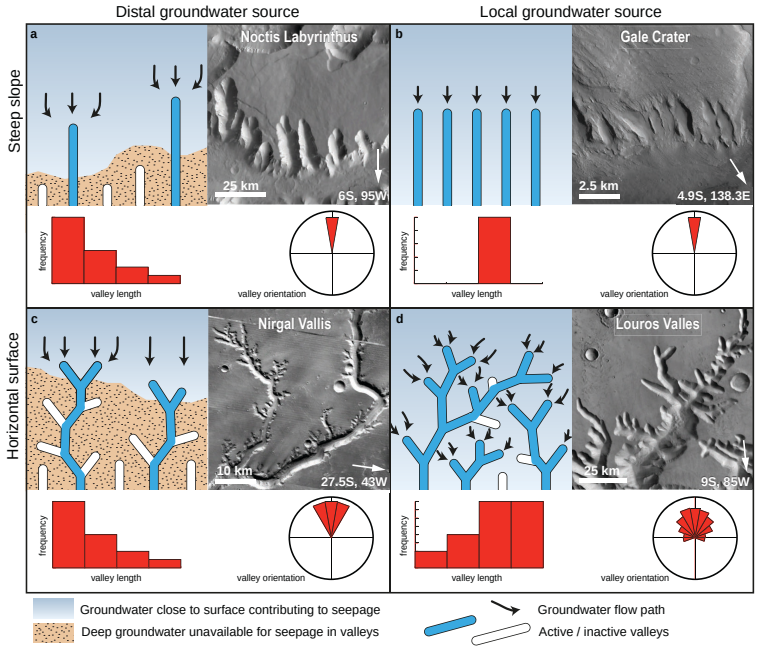

Figure 12. Landscape end-members formed by groundwater seepage as result from a distal or local source, and steep or horizontal surface. Each panel shows a schematic diagram (upper left), an Martian case showing a similar morphology (upper right) as an example and the expected valley length distribution and valley orientation (bottom). A distal source **(a, c)** results in valley abandonment due to upstream capture of groundwater, where a local groundwater source **(b, d)** is less prone to flow piracy. Horizontal surfaces **(c, d)** have a strong tendency to from valley bifurcations in contrast to steep slopes **(a, b)**. Distally-fed valleys result in an open landscape as no valleys develop downstream of large valleys. Similar Martian landscapes in **(a)** Noctis Labytinthus (THEMIS image), **(b)** Gale Crater (CTX image), **(c)** Nirgal Vallis (THEMIS image) and **(d)** Louros Valles (THEMIS image).

ESURFD
3, 129–171, 2015